

Estimating Longitudinal Polarization of Λ and $\bar{\Lambda}$ Hyperons at Relativistic Energies using Hydrodynamic and Transport models

Bhagyarathi Sahoo,^{*} Captain R. Singh,[†] and Raghunath Sahoo[‡]

Department of Physics, Indian Institute of Technology Indore, Simrol, Indore 453552, India

(Dated: December 31, 2024)

The global and local polarization measurements of Λ ($\bar{\Lambda}$) hyperons by STAR and ALICE Collaborations open up an immense interest in investigating the polarization dynamics in heavy-ion collisions. Recent studies suggest the transverse component of the vorticity field is responsible for the global spin polarization, while the longitudinal component of the vorticity field accounts for the local polarization. The local polarization of Λ -hyperons arises due to the anisotropic flows in the transverse plane, indicating a quadrupole pattern of the longitudinal vorticity along the beam direction. We derive a simple solution relating the longitudinal mean spin vector with the second-order anisotropic flow coefficient due to the thermal shear for an ideal uncharged fluid in a longitudinal boost invariant scenario. The present study focuses on the local (longitudinal) polarization of Λ and $\bar{\Lambda}$ in Au+Au and Pb+Pb collisions at $\sqrt{s_{NN}} = 200$ GeV and 5.02 TeV, respectively. Further, we explore the azimuthal angle, centrality, and transverse momentum (p_T) dependence study of longitudinal polarization using hydrodynamic and transport models. All these models predict a maximum longitudinal polarization in mid-central collisions around 30-50 % centrality at $p_T \approx 2.0 - 3.0$ GeV/c. These findings on longitudinal polarization advocate the existence of a thermal medium in non-central heavy-ion collisions.

I. INTRODUCTION

Recently, many studies have been conducted to investigate the physics involved in non-central ultra-relativistic heavy-ion collisions at the Relativistic Heavy Ion Collider (RHIC) and the Large Hadron Collider (LHC). The medium created in these collisions is believed to be the hottest, most dense, least viscous, and the most vortical fluid ever found in nature [1, 2]. The shear in the initial velocity distribution of the participants manifests a non-zero vorticity component, resulting in a net polarization of the produced particles along the orbital angular momentum (OAM) direction. This phenomenon is referred to as global polarization [3, 4]. Excluding OAM contribution, there are other sources contributing to vorticity. These include anisotropic flow, jet energy deposition, and deviations from longitudinal boost invariance in the transverse velocity fields [5–14]. Depending on the location of fluid elements within the created system, vorticity is generated in different directions, which could induce a local polarization of the particles.

At the early stages of the development of the relativistic spin-polarization framework, most relativistic hydrodynamic models assume the spin degrees of freedom in local thermodynamical equilibrium for studying global spin polarization. Consequently, a relationship emerges between spin polarization and thermal vorticity, suggesting polarization is directly proportional to the gradient of velocity and temperature

fields. Such polarization aligns with the direction of OAM. Besides global polarization, longitudinal (local) polarization of Λ -hyperons along the beam direction is observed in experiments [15–18]. The longitudinal polarization arises due to the inhomogeneous expansion of the fireball. Specifically, in non-central heavy-ion collisions, anisotropic flow in the transverse plane forms a quadrupole pattern of longitudinal vorticity along the beam direction (z-axis), leaving particles longitudinally polarized [5–10]. Unlike the polarization along OAM, the longitudinal polarization (P_z) is sensitive only to transverse expansion dynamics [8]. It does not decrease rapidly with increasing center-of-mass energy; thus, it is detectable even at LHC energies. Furthermore, it is sustained in the Bjorken longitudinal boost invariance scenario and does not require identifying the orientation of the reaction plane. However, the topology of the colliding ions plays a crucial role in determining the longitudinal polarization of the particles.

Over time, significant progress has been made in investigating the polarization of the particles in ultra-relativistic collisions [1, 3, 19–41]. There are numerous theoretical advancements, including Liang and Wang’s prediction of strange quark polarization caused by the spin-orbit coupling within the thermalized QCD matter [3]. Additionally, Becattini et al. proposed the global spin polarization of Λ -hyperons due to thermal vorticity [28]. Later, various theoretical frameworks based on 3+1D relativistic hydrodynamic and multiphase transport models were formulated to explain the global polarization of Λ -hyperons. Their predictions quantitatively and qualitatively agree with the experimental findings at the RHIC [1, 29–41]. This convergence of theory and experiment implies a need for a thorough study of longitudinal polarization of Λ -hyperons.

^{*} Bhagyarathi.Sahoo@cern.ch

[†] captainriturajsingh@gmail.com

[‡] Raghunath.Sahoo@cern.ch (corresponding author)

The experimental measurement of longitudinal polarization of Λ ($\bar{\Lambda}$) with the azimuthal angle (ϕ) relative to the second-order event plane (Ψ_2) by the STAR Collaboration [15, 16] shows an opposite trend as compared to the theoretical predictions [8]. This discrepancy between theoretical models and experimental data is commonly referred to as a “spin sign puzzle”. A study by Xie et al. employed a (3+1)D particle-in-cell relativistic hydrodynamic model, and the obtained results qualitatively agree with the experimental data [42]. Nonetheless, the reason for the disparate signs of longitudinal polarization across various hydrodynamic models remains uncertain. In some studies, it has been attempted to explain by adding a thermal shear term at local equilibrium into the spin polarization vector [43–47]. The authors have obtained the modified spin polarization vector in the linear response theory by assuming an isothermal decoupling hypersurface in local equilibrium and taking the linear order in the gradients of all thermodynamic fields. This modified spin polarization vector for spin-1/2 baryons contains contributions from kinematic vorticity and kinematic shear tensor. Using this definition of the spin polarization vector in the hydrodynamic model, the authors could reasonably explain the longitudinal polarization data [44]. Further, a multi-phase transport model (AMPT) based study was also able to address this polarization sign issue by considering the quadrupole structure of longitudinal vorticity [5].

Moreover, there have been several additional efforts to address this issue. For instance, by substituting the thermal vorticity in the spin polarization equation (Eq. 2) with projected thermal vorticity or T-vorticity, the longitudinal component of polarization flips its sign and aligns with experimental observations [48, 49]. Recently, Yi et al. estimated that the emergence of longitudinal polarization is due to a combination of shear-induced tensor, thermal vorticity, and fluid acceleration [50]. They argued that while the shear-induced term accounts for the correct angular dependence of longitudinal polarization, its overall impact might be nullified by thermal vorticity and fluid acceleration. Furthermore, Florkowski et al. examined the contributions of thermal shear and thermal vorticity to longitudinal polarization [51]. In their earlier work, they attempted to resolve this spin sign puzzle by incorporating a spin tensor component into the orbital angular momentum [52–55]. The spin sign puzzle has been attempted to solve by considering the gradient of chemical potential [56] and spin potential [57]. A chiral kinetic approach with AMPT initial conditions also predicts the same P_z modulation as experimental data [12]. This approach considers the transverse component of vorticity and non-equilibrium effects due to spin degrees of freedom.

However, the observation of longitudinal polarization of Λ -hyperons is not only limited to its azimuthal angle

dependence relative to the second-order event plane. The centrality, transverse momentum (p_T), and rapidity dependence of longitudinal polarization are also observed at the RHIC and LHC energies [15–18]. A simple boost-invariant blast wave (BW) hydrodynamic model with few freeze-out parameters explains the centrality and p_T dependence of longitudinal polarization measured at STAR Collaboration [15]. It considers the kinematic vorticity associated with the velocity field without contribution from the temperature gradients and acceleration term. Furthermore, a hydrodynamic model MUSIC with AMPT initial conditions is used to estimate the centrality, p_T and rapidity dependence of longitudinal polarization of Λ -hyperons. This MUSIC+AMPT-based study considers both thermal shear and thermal vorticity into account. It predicts the effect of thermal vorticity dominates over thermal shear when the longitudinal polarization of Λ and $\bar{\Lambda}$ hyperons is obtained at the freeze-out using hyperon mass as the mass of the spin carrier [17]. In other cases, using the strange quark mass in place of the hyperon mass, the effect of thermal shear dominates over thermal vorticity. As a consequence, it predicts positive longitudinal polarization, which is similar to the observed experimental data. So, the MUSIC+AMPT-based study advocates that Λ hyperons inherit the spin polarization of strange quarks. It is important to note that in both cases, the effect of hadronic interactions on Λ hyperons spin polarization is not considered. Therefore, the particle spin polarization dynamics depend on the assumptions used in the model to calculate the polarization observable. So, it is crucial to validate the longitudinal polarization data with other hydrodynamic and transport models that consider the hadronic scattering into account.

In the present work, we explore the longitudinal polarization due to the thermal shear tensor considering the temperature depends only on the Bjorken time for an ideal uncharged fluid. In the earlier work reported in Ref. [8], the authors have calculated the contribution of thermal vorticity on longitudinal polarization. Following Ref [8], we derive an analytical expression relating the longitudinal mean spin vector with the elliptic flow due to the symmetric thermal shear tensor. To obtain the local Λ -hyperon polarization under the developed formulation we have used hydrodynamic and multiphase transport models. The Eulerian Conservative High Order Quark Gluon Plasma (ECHO-QGP), and Energy conservation Parallel scattering factorization Saturation (EPOS4) models are used as a hydrodynamical-based approach and A MultiPhase Transport (AMPT) model is used as a kinetic theory-based approach to estimate the longitudinal polarization of Λ and $\bar{\Lambda}$ -hyperons. It is to be noted that the present study considers a longitudinal boost invariance scenario. Here, we investigate the azimuthal angle, centrality, and p_T dependence of longitudinal polarization of Λ -hyperons.

This paper is organized as follows. After a brief introduction in section I, we discuss the formulation of elliptic flow-induced local polarization in section II. Section III briefly describes the event generators, ECHO-QGP, EPOS4, and AMPT. The results obtained from the model are discussed in section IV. Finally, the important findings are summarized in section V.

II. METHODOLOGY

The total mean spin vector of a spin-1/2 particle at local thermodynamic equilibrium is the sum of the contribution that arises due to the thermal vorticity and thermal shear [43–45].

$$S^\mu(p) = S_\omega^\mu(p) + S_\xi^\mu(p) \quad (1)$$

where, $S_\omega^\mu(p)$ is the mean spin vector due to the thermal vorticity $\bar{\omega}$ and $S_\xi^\mu(p)$ is the mean spin vector due to the thermal shear ξ . In this section, we calculate the analytical expression for the longitudinal polarization for an ideal uncharged fluid due to the thermal vorticity and thermal shear in subsection II A and II B, respectively.

A. Thermal vorticity

The mean spin vector of a spin-1/2 particle, characterized by its four-momentum p , is intricately linked to the thermal vorticity at leading order [28, 29], and is given by;

$$S_\omega^\mu(p) = -\frac{1}{8m} \epsilon^{\mu\rho\sigma\tau} p_\tau \frac{\int_\Sigma d\Sigma_\lambda p^\lambda n_F (1 - n_F) \bar{\omega}_{\rho\sigma}}{\int_\Sigma d\Sigma_\lambda p^\lambda n_F}, \quad (2)$$

where $\bar{\omega}$ is the thermal vorticity, defined in terms of the anti-symmetric derivative of four temperature fields, given by;

$$\bar{\omega}_{\mu\nu} = -\frac{1}{2} (\partial_\mu \beta_\nu - \partial_\nu \beta_\mu) \quad (3)$$

The relation between four temperature vector, β^μ , and the four velocity u^μ , along with the temperature T , is expressed succinctly as $\beta^\mu = \frac{u^\mu}{T}$. This fundamental relationship, unveiled in Eq. (2), illuminates the decoupling hypersurface (Σ) dynamics. Within this domain, the covariant Fermi-Dirac phase space distribution function n_F is defined as $n_F = 1/[\exp(\beta \cdot p - \sum_j \mu_j q_j/T) + 1]$.

Further, it is assumed that under the vicinity of the ideal uncharged fluid the temperature vorticity,

$$\Omega_{\mu\nu} = \frac{1}{2} [\partial_\mu (T u_\nu) - \partial_\nu (T u_\mu)] \quad (4)$$

is conserved along the velocity i.e $\Omega_{\mu\nu} u^\nu = 0$ [4, 8] and satisfies the relativistic Kelvin circulation theorem. As a consequence, if $\Omega_{\mu\nu}$ vanishes at initial time, it remains absent during the whole evolution of the ideal uncharged fluid. Thus by using this condition, we can obtain the thermal vorticity, $\bar{\omega}$, given as [4, 8];

$$\bar{\omega}_{\mu\nu} = \frac{1}{T} (A_\mu u_\nu - A_\nu u_\mu) \quad (5)$$

here, A is the four-acceleration field.

Now, using the Eq. (5) in Eq. (2), one can obtain the modified form of the spin vector for spin-1/2 particles, which is given as;

$$S_\omega^\mu(p) = -\frac{1}{4m} \epsilon^{\mu\rho\sigma\tau} p_\tau \frac{\int_\Sigma d\Sigma_\lambda p^\lambda A_\rho \beta_\sigma n_F (1 - n_F)}{\int_\Sigma d\Sigma_\lambda p^\lambda n_F}, \quad (6)$$

For the ideal uncharged fluid, the equation of motion is defined as,

$$A_\rho = \frac{1}{T} \nabla_\rho T = \frac{1}{T} (\partial_\rho - u_\rho u \cdot \partial) T. \quad (7)$$

Replacing Eq. (7) in Eq. (6), we get;

$$S_\omega^\mu(p) = -\frac{1}{4mT} \epsilon^{\mu\rho\sigma\tau} p_\tau \left[\frac{\int_\Sigma d\Sigma_\lambda p^\lambda \partial_\rho T \beta_\sigma n_F (1 - n_F)}{\int_\Sigma d\Sigma_\lambda p^\lambda n_F} - \frac{\int_\Sigma d\Sigma_\lambda p^\lambda \beta_\sigma u_\rho u \cdot \partial T n_F (1 - n_F)}{\int_\Sigma d\Sigma_\lambda p^\lambda n_F} \right] \quad (8)$$

It must be noted that the inclusion of the term $\epsilon^{\mu\rho\sigma\tau} \beta_\sigma u_\rho$ in the second part of Eq. (8) results in this part becoming zero. Therefore, the spin polarization tensor is solely determined by the first term.

Now, with the help of the relation $\frac{\partial}{\partial p^\sigma} n_F = -\beta_\sigma n_F (1 - n_F)$, Eq. (8) is rewritten as;

$$S_\omega^\mu(p) = \frac{1}{4mT} \epsilon^{\mu\rho\sigma\tau} p_\tau \frac{\int_\Sigma d\Sigma_\lambda p^\lambda \frac{\partial n_F}{\partial p^\sigma} \partial_\rho T}{\int_\Sigma d\Sigma_\lambda p^\lambda n_F}, \quad (9)$$

By first solving the numerator of the above Eq. 9, we get

$$\int_\Sigma d\Sigma_\lambda p^\lambda \frac{\partial n_F}{\partial p^\sigma} \partial_\rho T = \frac{\partial}{\partial p^\sigma} \int_\Sigma d\Sigma_\lambda p^\lambda n_F \partial_\rho T - \int_\Sigma d\Sigma_\sigma n_F \partial_\rho T.$$

At the relativistic limit, it is assumed that the decoupling hypersurface happens at $T = T_c$, where T_c is the critical temperature. This entails that the normal vector

to the hypersurface is the gradient of temperature, which forces the second integral of the above expression to vanish. Then, the final expression for the mean spin vector is given by,

$$S_{\omega}^{\mu}(p) = \frac{1}{4mT} \epsilon^{\mu\rho\sigma\tau} p_{\tau} \frac{\partial}{\partial p^{\sigma}} \int_{\Sigma} d\Sigma_{\lambda} p^{\lambda} n_F \partial_{\rho} T \int_{\Sigma} d\Sigma_{\lambda} p^{\lambda} n_F \quad (10)$$

Here, we have considered an isochronous decoupling hypersurface, with a temperature field only dependent on the Bjorken time, τ . Further, the decoupling hypersurface is described by the coordinates x, y, η , with τ as a constant.

Let us calculate the numerator of Eq. (10) putting $\rho = 0$, we obtain;

$$\int_{\Sigma} d\Sigma_{\lambda} p^{\lambda} n_F \frac{dT}{d\tau} \cosh \eta. \quad (11)$$

Re-evaluating Eq. (10), at $Y = 0$, gives

$$S_{\omega}^z(\mathbf{p}_T, Y = 0) \hat{\mathbf{k}} \simeq -\frac{dT}{d\tau} \frac{1}{4mT} \hat{\mathbf{k}} \frac{\partial}{\partial \phi} \log \int_{\Sigma} d\Sigma_{\lambda} p^{\lambda} n_F \quad (12)$$

where ϕ is the azimuthal angle of the emitted particle in the transverse plane. Expanding the Eq. (12) in Fourier series in ϕ and keeping only the elliptic flow term produces a simplified form of the longitudinal component of the mean spin vector;

$$\begin{aligned} S_{\omega}^z(\mathbf{p}_T, Y = 0) &\simeq -\frac{dT}{d\tau} \frac{1}{4mT} \frac{\partial}{\partial \phi} 2v_2(p_T) \cos 2\phi \\ &= \frac{dT}{d\tau} \frac{1}{mT} v_2(p_T) \sin 2\phi \end{aligned} \quad (13)$$

In the rest frame of the particle, the longitudinal polarization vector P_z^* can be calculated from the longitudinal mean spin vector S_z^* by using the relation,

$$P_z^* = 2S_z^* \quad (14)$$

At the midrapidity, $S_z^* = S_z$.

The Eq. (13) implies that the degree of longitudinal polarization depends on the temperature cooling rate, the second-order anisotropic flow coefficient, and the azimuthal angle of the emitted particles. In peripheral heavy-ion collisions, the initial spatial anisotropy of the overlap region is converted into an anisotropic azimuthal distribution in the momentum space of the final state particles. This anisotropy can be characterized in terms of Fourier coefficients,

$$v_2 \equiv \langle \cos[2(\phi - \Psi_2)] \rangle \quad (15)$$

where Ψ_2 is the azimuthal angle of the event plane for the second-order harmonics.

B. Thermal shear

The mean spin vector of a spin-1/2 particle due to the thermal shear tensor is given by [43, 44];

$$S_{\xi}^{\mu}(p) = -\frac{1}{4m} \epsilon^{\mu\rho\sigma\tau} p_{\tau} \frac{\int_{\Sigma} d\Sigma \cdot p n_F (1 - n_F) \hat{t}_{\rho} \frac{p^{\lambda}}{\varepsilon} \xi_{\lambda\sigma}}{\int_{\Sigma} d\Sigma \cdot p n_F}, \quad (16)$$

where ξ is the thermal shear, defined in terms of the symmetric derivative of four temperature fields, given by;

$$\xi_{\mu\nu} = \frac{1}{2} (\partial_{\mu} \beta_{\nu} + \partial_{\nu} \beta_{\mu}) \quad (17)$$

here \hat{t}_{ρ} is the direction of QGP in the center of mass frame; $\varepsilon = \hat{t}_{\rho} \cdot p = \sqrt{p^2 + m^2}$ is the energy, and n_F is the Fermi Dirac distribution function.

Following these, thermal shear tensor can be written as;

$$\begin{aligned} \xi_{\mu\nu} &= \frac{1}{2} (\partial_{\mu} \beta_{\nu} + \partial_{\nu} \beta_{\mu}) = \frac{1}{T} \left[\frac{1}{2} (\partial_{\mu} u_{\nu} + \partial_{\nu} u_{\mu}) \right] \\ &\quad - \frac{1}{T^2} \left[\frac{1}{2} (u_{\nu} \partial_{\mu} T + u_{\mu} \partial_{\nu} T) \right] \end{aligned} \quad (18)$$

The symmetric shear tensor ($\Xi_{\mu\nu}$) can be decomposed as [43],

$$\Xi_{\mu\nu} = \frac{1}{2} (\partial_{\mu} u_{\nu} + \partial_{\nu} u_{\mu}) = \frac{1}{2} (A_{\mu} u_{\nu} + A_{\nu} u_{\mu}) + \sigma_{\mu\nu} + \frac{1}{3} \theta \Delta_{\mu\nu} \quad (19)$$

where A is the four acceleration field.

The shear stress tensor ($\sigma_{\mu\nu}$) in Eq. 19 can be written as;

$$\sigma_{\mu\nu} = \frac{1}{2} (\nabla_{\mu} u_{\nu} + \nabla_{\nu} u_{\mu}) - \frac{1}{3} \theta \Delta_{\mu\nu} \quad (20)$$

where $\theta = \partial_{\mu} u^{\mu}$ is the expansion rate, $\Delta^{\mu\nu} = g^{\mu\nu} - u^{\mu} u^{\nu}$ is the transverse projector operator, and defining the orthogonal derivative $\nabla_{\mu} = \Delta_{\mu\nu} \partial^{\nu} = \partial_{\mu} - u_{\mu} u \cdot \partial$

Further, the analytical expression for $\xi_{\mu\nu}$ from Eq. 18 is obtained as;

$$\begin{aligned} \xi_{\mu\nu} &= \frac{1}{2T} [(A_{\mu} u_{\nu} + A_{\nu} u_{\mu}) + (\nabla_{\mu} u_{\nu} + \nabla_{\nu} u_{\mu})] \\ &\quad - \frac{1}{2T^2} [(u_{\nu} \partial_{\mu} T + u_{\mu} \partial_{\nu} T)] \end{aligned} \quad (21)$$

Substituting the value of $\xi_{\lambda\sigma}$ in Eq. 16, the mean spin vector is proportional to;

$$\begin{aligned} S_{\xi}^{\mu}(p) &\propto \epsilon^{\mu\rho\sigma\tau} \frac{\hat{t}_{\rho}}{\varepsilon} p_{\tau} p^{\lambda} \left[\frac{1}{2T} [(A_{\lambda} u_{\sigma} + A_{\sigma} u_{\lambda}) + (\nabla_{\lambda} u_{\sigma} + \nabla_{\sigma} u_{\lambda})] \right. \\ &\quad \left. - \frac{1}{2T^2} [(u_{\sigma} \partial_{\lambda} T + u_{\lambda} \partial_{\sigma} T)] \right] \end{aligned} \quad (22)$$

Now, expanding the orthogonal derivative term in Eq. 22, we get;

$$S_\xi^\mu(p) \propto \epsilon^{\mu\rho\sigma\tau} \frac{\hat{t}_\rho}{\epsilon} p_\tau p^\lambda \left[\frac{1}{2T} [(A_\lambda u_\sigma + A_\sigma u_\lambda) + (\partial_\lambda u_\sigma - u_\lambda u \cdot \partial u_\sigma) + (\partial_\sigma u_\lambda - u_\sigma u \cdot \partial u_\lambda)] - \frac{1}{2T^2} (u_\sigma \partial_\lambda T + u_\lambda \partial_\sigma T) \right] \quad (23)$$

Further simplification of the above equation gives,

$$S_\xi^\mu(p) \propto \epsilon^{\mu\rho\sigma\tau} \frac{\hat{t}_\rho}{\epsilon} p_\tau \left[\frac{1}{2T} \left[(p \cdot A) u_\sigma + A_\sigma (p \cdot u) + ((p \cdot \partial) u_\sigma - (p \cdot u)(u \cdot \partial) u_\sigma) + (p^\lambda \partial_\sigma u_\lambda - p^\lambda u_\sigma u \cdot \partial u_\lambda) \right] - \frac{1}{2T^2} [(u_\sigma (p \cdot \partial) T + (p \cdot u) \partial_\sigma T)] \right] \quad (24)$$

Replacing acceleration four vector A defined in Eq. 7, the Eq. 24 can be transformed as,

$$S_\xi^\mu(p) \propto \epsilon^{\mu\rho\sigma\tau} \frac{\hat{t}_\rho}{\epsilon} p_\tau \left[\frac{1}{2T^2} [(p^\alpha (\partial_\alpha - u_\alpha u \cdot \partial) T) u_\sigma + (\partial_\sigma - u_\sigma u \cdot \partial) T (p \cdot u)] + \frac{1}{2T} \left[((p \cdot \partial) u_\sigma - (p \cdot u)(u \cdot \partial) u_\sigma) + (p^\lambda \partial_\sigma u_\lambda - p^\lambda u_\sigma u \cdot \partial u_\lambda) \right] - \frac{1}{2T^2} [(u_\sigma (p \cdot \partial) T + (p \cdot u) \partial_\sigma T)] \right] \quad (25)$$

Using the relation between four momentum and four velocity $p^\mu = mu^\mu$, and $p \cdot u = m$, we have

$$S_\xi^\mu(p) \propto \epsilon^{\mu\rho\sigma\tau} \frac{\hat{t}_\rho}{\epsilon} p_\tau \left[\frac{1}{2T^2} \left[(p \cdot \partial T - p \cdot \partial T) u_\sigma + (\partial_\sigma - u_\sigma u \cdot \partial) T (p \cdot u) \right] + \frac{1}{2T} \left[((p \cdot \partial) u_\sigma - (p \cdot \partial) u_\sigma) + (p^\lambda \partial_\sigma u_\lambda - p^\lambda u_\sigma u \cdot \partial u_\lambda) \right] - \frac{1}{2T^2} [(u_\sigma (p \cdot \partial) T + (p \cdot u) \partial_\sigma T)] \right] \quad (26)$$

With the help of the identity $u^\lambda \partial_\sigma u_\lambda = 0$; Eq. 26, reduces to;

$$S_\xi^\mu(p) \propto \epsilon^{\mu\rho\sigma\tau} \frac{\hat{t}_\rho}{2T^2 \epsilon} p_\tau \left[(\partial_\sigma T - u_\sigma u \cdot \partial T) (p \cdot u) - [(u_\sigma (p \cdot \partial) T + (p \cdot u) \partial_\sigma T)] \right] \quad (27)$$

Since we are considering the temperature field for Bjorken flow, the $\partial_\sigma T \rightarrow 0$. Hence Eq. 27, reduces to;

$$S_\xi^\mu(p) \propto \epsilon^{\mu\rho\sigma\tau} \frac{\hat{t}_\rho}{2T^2 \epsilon} p_\tau \left[-u_\sigma u \cdot \partial T (p \cdot u) - u_\sigma (p \cdot \partial) T \right] \quad (28)$$

On further simplification of $p \cdot u$ term, leads to;

$$S_\xi^\mu(p) \propto -\epsilon^{\mu\rho\sigma\tau} \frac{\hat{t}_\rho}{T \epsilon} p_\tau (p \cdot \partial T) \beta_\sigma \quad (29)$$

Substituting Eq. 29 in the Eq. 16, the mean spin vector can be written as,

$$S_\xi^\mu(p) = \frac{1}{4mT} \epsilon^{\mu\rho\sigma\tau} p_\tau \frac{\hat{t}_\rho \int_\Sigma d\Sigma \cdot p (p \cdot \partial T) n_F (1 - n_F) \beta_\sigma}{\int_\Sigma d\Sigma \cdot p n_F}, \quad (30)$$

Now, with the help of the relation $\frac{\partial}{\partial p^\sigma} n_F = -\beta_\sigma n_F (1 - n_F)$, Eq. (30) is rewritten as;

$$S_\xi^\mu(p) = \frac{-1}{4mT} \epsilon^{\mu\rho\sigma\tau} p_\tau \frac{\hat{t}_\rho \int_\Sigma d\Sigma \cdot p (p \cdot \partial T) \frac{\partial}{\partial p^\sigma} n_F}{\int_\Sigma d\Sigma \cdot p n_F}, \quad (31)$$

By solving the numerator of the above Eq. 31, we get

$$\int_\Sigma d\Sigma \cdot p \frac{\partial n_F}{\partial p^\sigma} (p \cdot \partial T) = \frac{\partial}{\partial p^\sigma} \int_\Sigma d\Sigma \cdot p n_F (p \cdot \partial T) - \int_\Sigma d\Sigma \cdot p n_F \partial_\sigma T - \int_\Sigma d\Sigma_\sigma n_F (p \cdot \partial T) \quad (32)$$

The second and third integral of the above equation vanishes with a similar argument as discussed above. Thus, Eq. 31, becomes;

$$S_\xi^\mu(p) = \frac{-1}{4mT} \epsilon^{\mu\rho\sigma\tau} p_\tau \frac{\hat{t}_\rho \frac{\partial}{\partial p^\sigma} \int_\Sigma d\Sigma \cdot p n_F (p \cdot \partial T)}{\int_\Sigma d\Sigma \cdot p n_F}, \quad (33)$$

At $\rho = 0$, the numerator of Eq. 33, is given as;

$$\int_\Sigma d\Sigma \cdot p n_F \epsilon \frac{dT}{dT} \cosh \eta. \quad (34)$$

Hence, at $Y = 0$, the $\cosh\eta \approx 1$.

$$S_{\xi}^{\mu}(p) = \frac{-1}{4mT} \epsilon^{\mu\rho\sigma\tau} p_{\tau} \frac{\partial}{\partial p^{\sigma}} \int_{\Sigma} d\Sigma \cdot p n_F \frac{dT}{d\tau}, \quad (35)$$

Eq. 35, follows the same form as Eq. 10. Hence the net contribution to the mean spin vector due to the thermal shear term is obtained as;

$$S_{\xi}^z(\mathbf{p}_T, Y = 0) \hat{\mathbf{k}} \simeq \frac{1}{4mT} \frac{dT}{d\tau} \hat{\mathbf{k}} \frac{\partial}{\partial \phi} \log \int_{\Sigma} d\Sigma_{\lambda} p^{\lambda} n_F \quad (36)$$

Expanding the Eq. (36) in Fourier series in ϕ and keeping only the elliptic flow term produces a simplified form of the longitudinal component of the mean spin vector;

$$\begin{aligned} S_{\xi}^z(\mathbf{p}_T, Y = 0) &\simeq \frac{1}{4mT} \frac{dT}{d\tau} \frac{\partial}{\partial \phi} 2v_2(p_T) \cos 2\phi \\ &= \frac{-1}{mT} \frac{dT}{d\tau} v_2(p_T) \sin 2\phi \end{aligned} \quad (37)$$

We found that the contribution of thermal shear on the mean spin vector is exactly equal but with an opposite sign for an ideal uncharged fluid assuming the temperature evolution only with the Bjorken time.

In this study, the second-order anisotropic flow coefficient (elliptic flow) is obtained using ECHO-QGP, EPOS4, and the AMPT model. The hydrodynamic temperature evolution is obtained using the (3+1)D relativistic hydrodynamic model. In this work, the event-by-event elliptic flow coefficient is obtained using the event plane method [58]. A brief description of ECHO-QGP, EPOS4, and AMPT models and event generation using these models is provided in section III.

III. EVENT GENERATION AND DESCRIPTION OF THE MODEL

Computational frameworks based on the modeling of theoretical physics with some approximation are commonly called ‘‘event generators’’. These event generators play a crucial role in comprehending the physics of ultra-relativistic A–A, p –A, and p – p collisions. At the fundamental level, these essential computational tools facilitate the connection between theoretical models and experimental data. As mentioned, the present study uses ECHO-QGP, EPOS4, and AMPT event generators to estimate longitudinal polarization at ultra-relativistic heavy-ion collisions using elliptic flow and azimuthal angle of emitted particles. A brief introduction about these generators is provided in this section for completeness.

A. ECHO-QGP

ECHO-QGP is a relativistic hydrodynamic model used to study the dynamics of heavy-ion collisions. Here, we have used the setup of the ECHO-QGP with Israel-Stewart (IS) based (3+1)-D viscous hydrodynamics model along Bjorken coordinates. In this study, we consider both shear and bulk viscosity to be finite, and these two viscosities are related to the squared speed of sound. The value of shear viscosity to entropy density ratio is mentioned in Table I. The initial conditions are obtained from the geometric Glauber model based on the energy density parameter. The parameters used to estimate the flow coefficients and, hence, the polarization in ECHO-QGP are discussed in Table I. For the present study, we have taken the kinetic freeze-out temperature as 120 MeV for Au+Au collisions at $\sqrt{s_{NN}} = 200$ GeV and Pb+Pb collisions at $\sqrt{s_{NN}} = 5.02$ TeV as both of them are found to be nearly equal in the blast wave framework [59] and our results don’t change appreciably within a variation of 20 MeV freeze-out temperature. The equation of state (EOS) of the system is a must to solve hydrodynamic equations. Although ECHO-QGP uses various EOS to describe the hydrodynamic evolution of the system, however in our study, we used the most realistic partial chemical equilibrium (PCE) EOS, which includes the comprehensive chemical composition of the hadronic species before the kinetic freeze-out. The freeze-out procedure is based on the Cooper-Frye formalism. The ECHO-QGP succeeded in explaining the transverse momentum spectra and anisotropic flow coefficients (mostly the elliptic flow) in central and mid-central collisions in the p_T range up to 1.5 - 2.0 GeV/c for the produced hadrons [60, 61]. The detailed description and formalism implemented in the model can be found in Ref [62]. The present study considers that hydrodynamic evolution occurs in a baryon-free region, it also neglects all possible electromagnetic effects and other possible fluctuations in the medium.

B. EPOS4

The EPOS4 is an updated version of the Monte-Carlo event generator named EPOS [63, 64]. EPOS4 is developed with an array of unbiased parallel multiple-scattering formalisms. It incorporates the classical Gribov-Regge framework and the modern Dokshitzer-Gribov-Lipatov-Altarelli-Parisi (DGLAP) formalism. This amalgamation captures the parallel scattering within the S-matrix theory and characterizes the perturbative approach and saturation effects. Further, EPOS4 reproduces the perfect factorization and binary scaling in AA collisions by simultaneously considering the rigorous parallel scattering, energy-momentum sharing, AGK theorem, and factorization for hard processes by introducing saturation. In its description of hadronization, EPOS4 adopts a core-corona paradigm, where

TABLE I. Parameter set used within the ECHO-QGP freeze-out routine.

System	$\sqrt{s_{NN}}$ (GeV)	σ_{NN} (mb)	τ_0 (fm/c)	e_0 (GeV/fm) ³	α	η/s	τ_π	Δ_η	σ_η	T_{freeze} (GeV)
Au+Au	200	40	0.6	24.5	1.0	0.1	3.0	3.0	1.0	0.120
Pb+Pb	5020	70	0.4	60.0	1.0	0.1	3.0	3.0	1.0	0.120

the high string density core hadronizes statistically while the low string density corona uses Lund string fragmentation [64]. The mechanism of the core-corona approach, which starts after some initial time $\tau_0 = 0.4$ fm/c, has been discussed in detail in Ref. [65]. The hot and dense QCD matter with low- p_T pre-hadrons, the “core”, evolves with the (3+1)D viscous hydrodynamics using vHILL [66]. It employs a straightforward crossover EOS calibrated with lattice QCD data [63]. Based on the micro-canonical approach, as the system expands and cools down, it reaches the hadronization point at energy density $\epsilon_H \approx 0.57$ GeV/fm³. Meanwhile, pre-hadrons with high- p_T traverse through the core and form the “corona”. However, these may still re-interact with the core hadrons through hadronic scatterings. The succeeding interactions between the formed hadrons are incorporated by employing the UrQMD as an after-burner. We have simulated a minimum bias of 2×10^6 events for Pb+Pb collisions at $\sqrt{s_{NN}} = 5.02$ TeV, and 6×10^6 events for Au+Au collisions at $\sqrt{s_{NN}} = 200$ GeV using EPOS4.

C. AMPT

A multi-phase transport model (AMPT) is a comprehensive approach that combines both initial partonic collisions and final hadronic interactions, effectively accounting for the transition between these distinct phases of matter. It is divided into four major components: first, the initialization of collisions is processed through the HIJING model [67], parton transport is executed using the Zhang Parton Cascade (ZPC) model [68], hadronization is based on the quark coalescence mechanism in string melting mode [69], and at last, hadron transport is conducted through a relativistic transport model (ART). Detailed descriptions of these models and their components are given in Ref. [70]. In the present study, we employ the string melting mode of AMPT for event generation as it effectively explains the anisotropic flow and particle spectra in the intermediate- p_T region, aligning with predictions provided by quark coalescence mechanism for hadronization [71–73]. To calculate the elliptic flow using AMPT, we adopted the averaged initial state from the Monte Carlo Glauber model, with parameters specified in Ref. [74]. The AMPT settings utilized are consistent with those reported in Refs. [75] for heavy-ion collisions at LHC and RHIC energies. For our purpose, we generated 2×10^6 minimum bias events for Pb+Pb collisions at $\sqrt{s_{NN}} = 5.02$ TeV, and 6×10^6 events for Au+Au col-

lisions at $\sqrt{s_{NN}} = 200$ GeV, employing identical settings within the AMPT framework.

IV. RESULTS AND DISCUSSION

In this work, we estimate the longitudinal polarization vector (P_z) of Λ ($\bar{\Lambda}$) hyperons as a function of azimuthal angle (ϕ), collision centrality, and transverse momentum (p_T). The longitudinal mean spin vector due to the thermal vorticity and thermal shear are given in Eq. 13 and Eq. 37, respectively. The longitudinal polarization depends on the decoupling hypersurface temperature, temperature gradient at hadronization, second-order anisotropic flow co-efficient (i.e., the elliptic flow), mass, and the sine of the azimuthal angular distribution of emitted Λ ($\bar{\Lambda}$) hyperons. We use a realistic 3+1 D viscous hydrodynamic ECHO-QGP, EPOS4, and a hybrid transport AMPT model to simulate heavy-ion collisions. Using these models, we obtain the elliptic flow and the azimuthal angle of emitted Λ ($\bar{\Lambda}$) hyperons. The hydrodynamic temperature evolution at hadronization is obtained from the ECHO-QGP. In EPOS4, the elliptic flow coefficient is obtained using Eq 15. However, in AMPT and ECHO-QGP, there is a provision for making the reaction plane angle $\Psi_2 = 0$, although it is nontrivial in experiments. Thus, one can obtain the elliptic flow coefficients as $v_2 = \langle \cos 2\phi \rangle$, here, the average is taken over all Λ produced in an event. The choice of centrality selection in the ECHO-QGP model is obtained for fixed impact parameter values based on Monte-Carlo Glauber model estimation [74]. However, for EPOS4 and AMPT models, the centrality selection is performed with the geometrical slicing of the impact parameter distribution.

Figure 1 shows P_z as a function of ϕ for Λ -hyperons obtained using the ECHO-QGP hydrodynamic model simulation. The green solid and dashed line shows P_z due to the thermal vorticity and the thermal shear, respectively, in Pb+Pb collisions at $\sqrt{s_{NN}} = 5.02$ TeV for (30-50)% with p_T range $0.15 < p_T < 3.0$ GeV/c. Similarly, the red solid and dashed line shows the P_z due to the thermal vorticity and the thermal shear, respectively, for Au+Au collisions at $\sqrt{s_{NN}} = 200$ GeV with the same p_T and centrality classes. Figure 1 indicates the sine modulation of P_z with ϕ . The value of P_z due to the thermal shear and thermal vorticity are found to be exactly equal with an opposite sign. A similar observation is reported in Refs. [50, 51]. It is evident that considering the thermal shear in place of

thermal vorticity qualitatively reproduces the correct sign of sine modulation of longitudinal polarization as observed at STAR experiment [15]. Similarly, Fig. 2 shows P_z as a function of ϕ for three different models used in the study for Pb+Pb collisions at (30-50)% centrality class and p_T range $0.15 < p_T < 3.0$ GeV/c. A very marginal difference in P_z as a function of ϕ is found between the hydrodynamic and transport models.

It is noteworthy to mention that the contribution of thermal shear and thermal vorticity on longitudinal mean spin vector are exactly equal in magnitude but an opposite sign is obtained only using the equation of motion for an ideal uncharged fluid. This simple solution of relating the longitudinal mean spin vector with elliptic flow is obtained by assuming the temperature evolution only with the Bjorken time. However, considering the temperature gradient, chemical potential gradient, and electromagnetic field terms in the mean spin vector, a finite longitudinal polarization is expected.

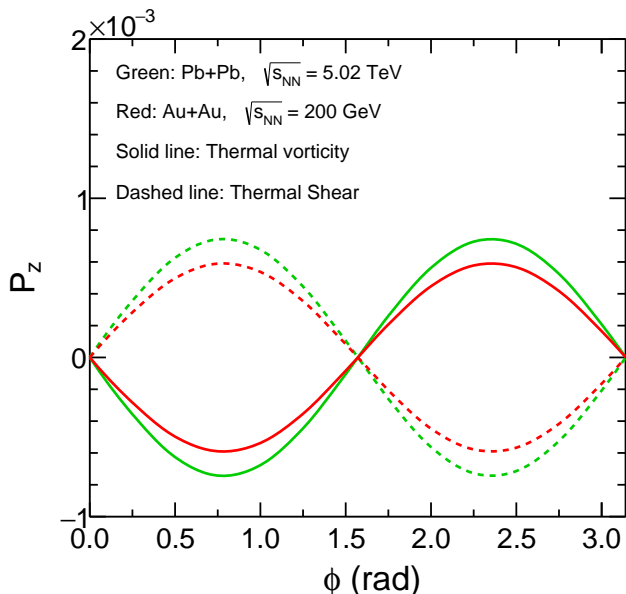


FIG. 1. (Color online) The longitudinal component of Λ and $\bar{\Lambda}$ polarization (P_z) as a function of azimuthal angle (ϕ) obtained from ECHO-QGP model simulation for $\sqrt{s_{NN}} = 5.02$ TeV and $\sqrt{s_{NN}} = 200$ GeV in Pb+Pb and Au+Au collisions, respectively.

The centrality dependence of P_z for Λ -hyperons obtained from hydrodynamic and transport models is shown in Fig. 3 for p_T range $0.15 < p_T < 3.0$ GeV/c in Au+Au collisions at $\sqrt{s_{NN}} = 200$ GeV and Pb+Pb collisions at $\sqrt{s_{NN}} = 5.02$ TeV, taking only thermal vorticity contribution. The positive P_z shown in Fig. 3 is the manifestation of two negative signs appearing in Eq.(11); one is from temperature cooling rate, and the other one is from $\sin 2\phi$. The term $\sin 2\phi$ in Eq. 13 is calculated by taking the sine of the average over all azimuthal angles

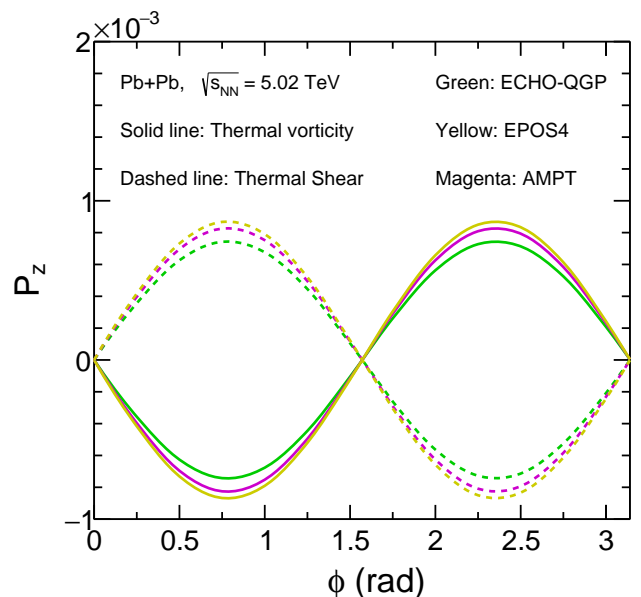


FIG. 2. (Color online) The longitudinal component of Λ and $\bar{\Lambda}$ polarization (P_z) as a function of azimuthal angle (ϕ) obtained from ECHO-QGP, EPOS4, AMPT model simulation for $\sqrt{s_{NN}} = 5.02$ TeV in Pb+Pb collisions.

carried by the Λ hyperons produced in an event. It is observed that the magnitude of longitudinal polarization increases from most-central to mid-central collisions. The observed increase in signal with decreasing centrality can be attributed to the rising contributions of elliptic flow in peripheral collisions. In most central collisions, the polarization seems to disappear, whereas in such collisions, the elliptic flow might be significant due to the initial density fluctuations.

ECHO-QGP predicts a slightly higher value of P_z in top (0-30)% central Au+Au collisions at $\sqrt{s_{NN}} = 200$ GeV compared to the Pb+Pb collision at $\sqrt{s_{NN}} = 5.02$ TeV. Furthermore, around (30-50)% mid-central collisions, the degree of longitudinal polarization obtained from the ECHO-QGP model dominates for Pb+Pb collisions compared to the Au+Au collisions. The AMPT model predicts a slightly higher value of P_z for Pb+Pb, $\sqrt{s_{NN}} = 5.02$ TeV as compared with the Au+Au, $\sqrt{s_{NN}} = 200$ GeV for all centrality classes. The trend of longitudinal polarization with centrality for EPOS4 is the same as AMPT, though both are based on different formulations. The current formulation integrated with AMPT and EPSO4 predicts change in the magnitude of polarization, P_z for Λ and $\bar{\Lambda}$, with center-of-mass energy ($\sqrt{s_{NN}}$). However, ECHO-QGP based results for the P_z of Λ and $\bar{\Lambda}$ are inconsistent with $\sqrt{s_{NN}}$. The small variations between the hydrodynamic and transport models arise due to different evolution and hadronization processes considered in these models. Here, we have observed that the magnitude of the collision center of the mass-energy dependence of elliptic flow-induced polarization along the beam direction

is weak as compared to the global spin polarization reported in Ref. [1].

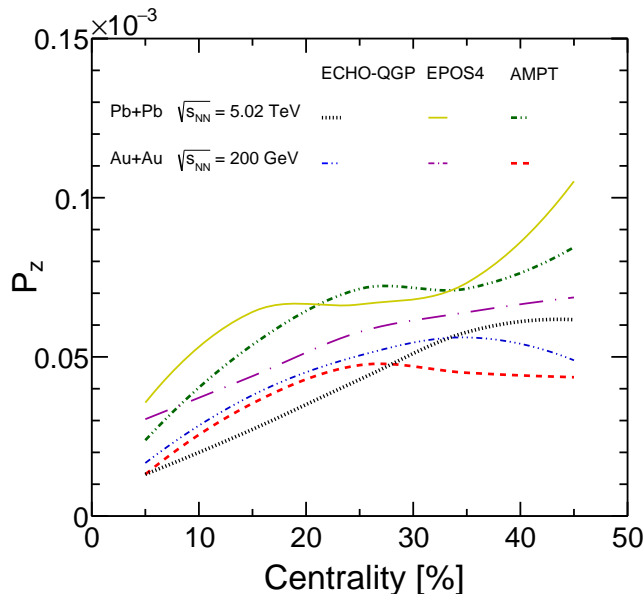


FIG. 3. (Color online) The longitudinal component of Λ and $\bar{\Lambda}$ polarization (P_z) as a function of collision centrality obtained from ECHO-QGP, EPOS4, and AMPT model simulation for $\sqrt{s_{NN}} = 5.02$ TeV and $\sqrt{s_{NN}} = 200$ GeV in Pb+Pb and Au+Au collisions, respectively.

Since the elliptic flow depends on the centrality and p_T , the polarization along the beam direction also exhibits the p_T dependence. Figure 4 indicates a p_T dependence of the elliptic flow-induced polarization for Λ ($\bar{\Lambda}$) hyperons in (30-50)% centrality bin by taking only the thermal vorticity contribution. It is observed that the longitudinal polarization increases for $p_T \lesssim 2.0$ GeV/c and decreases towards $p_T \gtrsim 2.0$ GeV/c for ECHO-QGP. Further, the ECHO-QGP predicts the negative longitudinal polarization at low p_T for Pb+Pb collisions. Because the elliptic flow obtained from ECHO-QGP has negative values for Λ ($\bar{\Lambda}$) hyperons at low $-p_T$. While, for AMPT, P_z increases with p_T , and this increasing trend of beam-induced polarization as a function of p_T is due to the elliptic flow behavior obtained from the AMPT. For EPOS4, P_z exhibits a non-monotonic behavior for Λ ($\bar{\Lambda}$) hyperons with p_T .

V. SUMMARY

In summary, we estimate the longitudinal component of polarization for Λ and $\bar{\Lambda}$ hyperons in Au+Au collisions at $\sqrt{s_{NN}} = 200$ GeV and Pb+Pb collisions at $\sqrt{s_{NN}} = 5.02$ TeV. We use a 3+1 D relativistic viscous hydrodynamic models such as ECHO-QGP, EPOS4, and a hybrid transport AMPT model to investigate the polarization along the beam direction. We obtain the longi-

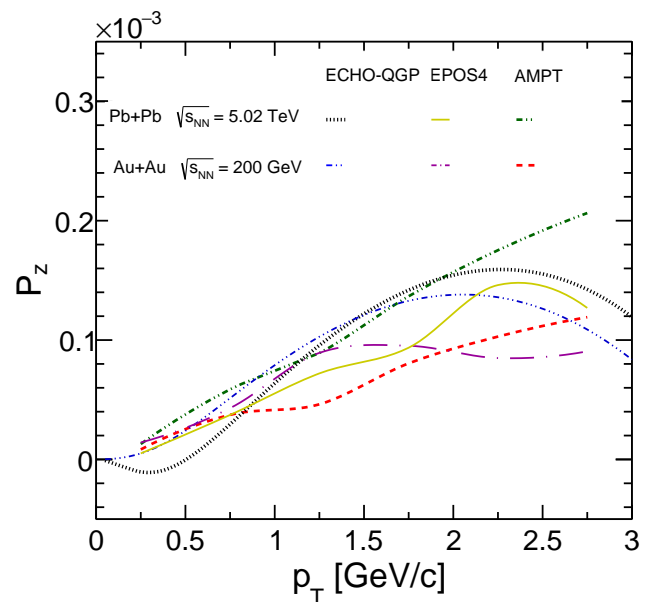


FIG. 4. (Color online) The longitudinal component of Λ and $\bar{\Lambda}$ polarization (P_z) as a function of transverse momentum (p_T) obtained from ECHO-QGP, EPOS4, and AMPT model simulation for $\sqrt{s_{NN}} = 5.02$ TeV and $\sqrt{s_{NN}} = 200$ GeV in Pb+Pb and Au+Au collisions, respectively for (30-50)% centrality classes.

tudinal polarization from the elliptic flow coefficients in a longitudinal boost scenario with no initial state fluctuations. We assume the spin degrees of freedom are in local thermodynamic equilibrium with the ideal fluid. This study is sensitive to the chosen initial conditions for the hydrodynamic and transport models simulation and the temperature gradient at the decoupling stage. The results show a centrality dependence of longitudinal polarization with increasing magnitude from most-central to mid-central collisions, which tends to decrease towards peripheral collisions. We observe a transverse momentum dependence of longitudinal polarization in both systems at relativistic energies. It is observed that the longitudinal polarization increases with $p_T \lesssim 2.0$ GeV/c and seems to decrease towards $p_T \gtrsim 2.0$ GeV/c.

The longitudinal polarization obtained in this study is due to the second-order anisotropic flow coefficients showing the quadrupole structure of the vorticity field in the transverse plane. However, the higher-order anisotropic flow harmonics also have similar vorticity structures in the transverse plane and contribute to the longitudinal polarization. Recently, the STAR Collaboration reported such observation in Ref. [18]. The sine modulation of P_z relative to the third-order event plane exhibits a sextupole pattern of vorticity induced by triangular flow in isobar collisions. It is important to note that the contribution of axial chemical potential and electromagnetic field in the mean spin vector are not taken into consideration in the present study. Apart from these, there could be various other factors that

affect the local spin polarization of Λ hyperons. Such as the feed-down of higher excited states and considering particle spin as an independent degree of freedom in each stage of the relativistic spin magneto-hydrodynamic framework may provide a comprehensive understanding of the local polarization.

More insightful investigations are required to comprehensively understand the global and/or local quark spin polarization in the QGP medium. These studies may comprise the spin-transfer mechanism at the hadronization stage, the relaxation time required to convert the vorticity to particle polarization, the effect of hadronic rescattering on the spin polarization, etc. With the current Run 3 high statistics data samples of ALICE, more differential and precision measurements can be performed on the local and global polarization of single and multi-strange baryons. With the precise vertexing and low p_T measurement capabilities for heavy flavor hadrons in Run 3 of ALICE, it would be interesting to investigate the global and local polarization dynamics of heavy flavor hadrons. This may reveal some of the open questions, such as: (i) Are the heavy flavor hadrons thermalized with the medium? (ii) Is the polarization achieved at the quark-gluon plasma phase or the hadronic phase? (iii) Does the hadron

polarization depend upon the quantum number of the constituent quark species?

ACKNOWLEDGEMENT

The authors would like to acknowledge some fruitful discussions with Ronald Scaria and Suraj Prasad during the preparation of the manuscript. Bhagyarathi Sahoo acknowledges the financial aid from CSIR, Government of India. The authors gratefully acknowledge the DAE-DST, Government of India funding under the mega-science project "Indian Participation in the ALICE experiment at CERN" bearing Project No. SR/MF/PS-02/2021-IITI (E-37123).

-
- [1] L. Adamczyk *et al.* [STAR Collaboration], *Nature* **548** 62 (2017).
- [2] J. E. Bernhard, J. S. Moreland and S. A. Bass, *Nature Phys.* **15** 1113 (2019).
- [3] Z. T. Liang and X. N. Wang, *Phys. Rev. Lett.* **94**, 102301 (2005) [erratum: *Phys. Rev. Lett.* **96**, 039901 (2006)].
- [4] F. Becattini, G. Inghirami, V. Rolando, A. Beraudo, L. Del Zanna, A. De Pace, M. Nardi, G. Pagliara and V. Chandra, *Eur. Phys. J. C* **75**, 406 (2015) [erratum: *Eur. Phys. J. C* **78**, 354 (2018)].
- [5] X. L. Xia, H. Li, Z. B. Tang and Q. Wang, *Phys. Rev. C* **98**, 024905 (2018).
- [6] Y. Jiang, Z. W. Lin and J. Liao, *Phys. Rev. C* **94**, 044910 (2016); **95**, 049904(E) (2017).
- [7] D. X. Wei, W. T. Deng and X. G. Huang, *Phys. Rev. C* **99**, 014905 (2019).
- [8] F. Becattini and I. Karpenko, *Phys. Rev. Lett.* **120**, 012302 (2018).
- [9] S. A. Voloshin, *EPJ Web Conf.* **171**, 07002 (2018).
- [10] L. G. Pang, H. Petersen, Q. Wang and X. N. Wang, *Phys. Rev. Lett.* **117**, 192301 (2016).
- [11] B. Betz, M. Gyulassy and G. Torrieri, *Phys. Rev. C* **76**, 044901 (2007).
- [12] Y. Sun and C. M. Ko, *Phys. Rev. C* **99**, 011903 (2019).
- [13] B. Sahoo, C. R. Singh, D. Sahu, R. Sahoo and J. e. Alam, *Eur. Phys. J. C* **83**, 873 (2023).
- [14] K. K. Pradhan, B. Sahoo, D. Sahu and R. Sahoo, *Eur. Phys. J. C* **84**, 936 (2024).
- [15] J. Adam *et al.* [STAR Collaboration], *Phys. Rev. Lett.* **123**, 132301 (2019).
- [16] T. Niida [STAR Collaboration], *Nucl. Phys. A* **982**, 511 (2019).
- [17] S. Acharya *et al.* [ALICE Collaboration], *Phys. Rev. Lett.* **128**, 172005 (2022).
- [18] M. Abdulhamid *et al.* [STAR Collaboration], *Phys. Rev. Lett.* **131**, 202301 (2023).
- [19] Z. T. Liang and X. N. Wang, *Phys. Lett. B* **629**, 20 (2005).
- [20] F. Becattini, L. Csernai and D. J. Wang, *Phys. Rev. C* **88**, 034905 (2013) [erratum: *Phys. Rev. C* **93**, 069901 (2016)].
- [21] F. Becattini, G. Cao and E. Speranza, *Eur. Phys. J. C* **79**, 741 (2019).
- [22] I. Karpenko and F. Becattini, *Eur. Phys. J. C* **77**, 213 (2017).
- [23] Y. L. Xie, M. Bleicher, H. Stöcker, D. J. Wang and L. P. Csernai, *Phys. Rev. C* **94**, 054907 (2016).
- [24] F. Becattini, *Rept. Prog. Phys.* **85**, 122301 (2022).
- [25] Y. Hidaka, S. Pu, Q. Wang and D. L. Yang, *Prog. Part. Nucl. Phys.* **127**, 103989 (2022).
- [26] B. Sahoo, D. Sahu, S. Deb, C. R. Singh and R. Sahoo, *Phys. Rev. C* **109**, 034910 (2024).
- [27] B. Sahoo, C. R. Singh and R. Sahoo, [arXiv:2402.17344 [hep-ph]].
- [28] F. Becattini, V. Chandra, L. Del Zanna and E. Grossi, *Annals Phys.* **338** 32 (2013).
- [29] R. H. Fang, L. G. Pang, Q. Wang and X. N. Wang, *Phys. Rev. C* **94**, 024904 (2016).
- [30] H. Li, L. G. Pang, Q. Wang and X. L. Xia, *Phys. Rev. C* **96**, 054908 (2017).

- [31] B. Fu, K. Xu, X. G. Huang and H. Song, Phys. Rev. C **103**, 024903 (2021).
- [32] S. Alzhrani, S. Ryu and C. Shen, Phys. Rev. C **106**, 014905 (2022).
- [33] I. Karpenko and F. Becattini, Nucl. Phys. A **967**, 764 (2017).
- [34] O. Vitiuk, L. V. Bravina and E. E. Zabrodin, Phys. Lett. B **803**, 135298 (2020).
- [35] Y. Sun and C. M. Ko, Phys. Rev. C **96**, 024906 (2017).
- [36] Y. B. Ivanov, V. D. Toneev and A. A. Soldatov, Phys. Rev. C **100**, 014908 (2019).
- [37] F. Becattini and M. A. Lisa, Ann. Rev. Nucl. Part. Sci. **70**, 395 (2020).
- [38] Y. Xie, D. Wang and L. P. Csernai, Phys. Rev. C **95**, 031901 (2017).
- [39] H. Li, H. Petersen, L. G. Pang, Q. Wang, X. L. Xia and X. N. Wang, Nucl. Phys. A **967**, 772 (2017).
- [40] J. Adam *et al.* [STAR Collaboration], Phys. Rev. C **98**, 014910 (2018).
- [41] S. Acharya *et al.* [ALICE Collaboration], Phys. Rev. C **101**, 044611 (2020). [erratum: Phys. Rev. C **105**, 029902 (2022)]
- [42] Xie, Y., Wang, D. and Csernai, L.P., Eur. Phys. J. C **80**, 39 (2020).
- [43] F. Becattini, M. Buzzegoli and A. Palermo, Phys. Lett. B **820**, 136519 (2021).
- [44] F. Becattini, M. Buzzegoli, G. Inghirami, I. Karpenko and A. Palermo, Phys. Rev. Lett. **127**, 272302 (2021).
- [45] A. Palermo, E. Grossi, I. Karpenko and F. Becattini, Eur. Phys. J. C **84**, 920 (2024).
- [46] S. Y. F. Liu and Y. Yin, JHEP **07**, 188 (2021).
- [47] B. Fu, S. Y. F. Liu, L. Pang, H. Song and Y. Yin, Phys. Rev. Lett. **127**, 142301 (2021).
- [48] W. Florkowski, A. Kumar, R. Ryblewski and A. Mazeliauskas, Phys. Rev. C **100**, 054907 (2019).
- [49] H. Z. Wu, L. G. Pang, X. G. Huang and Q. Wang, Phys. Rev. Research. **1**, 033058 (2019).
- [50] C. Yi, S. Pu and D. L. Yang, Phys. Rev. C **104**, 064901 (2021).
- [51] W. Florkowski, A. Kumar, A. Mazeliauskas and R. Ryblewski, Phys. Rev. C **105**, 064901 (2022).
- [52] W. Florkowski, B. Friman, A. Jaiswal and E. Speranza, Phys. Rev. C **97**, 041901 (2018).
- [53] W. Florkowski, B. Friman, A. Jaiswal, R. Ryblewski and E. Speranza, Phys. Rev. D **97**, 116017 (2018).
- [54] S. Bhadury, W. Florkowski, A. Jaiswal, A. Kumar and R. Ryblewski, Phys. Lett. B **814**, 136096 (2021).
- [55] S. Bhadury, W. Florkowski, A. Jaiswal, A. Kumar and R. Ryblewski, Phys. Rev. D **103**, 014030 (2021).
- [56] S. Y. F. Liu and Y. Yin, Phys. Rev. D **104**, 054043 (2021).
- [57] M. Buzzegoli, Phys. Rev. C **105**, 044907 (2022).
- [58] M. Masera, G. Ortona, M. G. Poghosyan and F. Prino, Phys. Rev. C **79**, 064909 (2009).
- [59] Studying the Phase Diagram of QCD Matter at RHIC (STAR Collaboration), https://drupal.star.bnl.gov/STAR/files/BES_WPII_ver6.9_Cover.pdf
- [60] T. Hirano, P. Huovinen and Y. Nara, Phys. Rev. C **84**, 011901 (2011).
- [61] X. F. Chen, T. Hirano, E. Wang, X. N. Wang and H. Zhang, Phys. Rev. C **84**, 034902 (2011).
- [62] L. Del Zanna, V. Chandra, G. Inghirami, V. Rolando, A. Beraudo, A. De Pace, G. Pagliara, A. Drago and F. Becattini, Eur. Phys. J. C **73**, 2524 (2013).
- [63] K. Werner, B. Guiot, I. Karpenko and T. Pierog, Phys. Rev. C **89**, 064903 (2014).
- [64] T. Pierog, I. Karpenko, J. M. Katzy, E. Yatsenko and K. Werner, Phys. Rev. C **92**, 034906 (2015).
- [65] K. Werner, Phys. Rev. C **109**, 014910 (2024).
- [66] I. Karpenko, P. Huovinen and M. Bleicher, Comput. Phys. Commun. **185**, 3016 (2014).
- [67] X. N. Wang and M. Gyulassy, Phys. Rev. D **44**, 3501 (1991).
- [68] B. Zhang, Comput. Phys. Commun. **109**, 193 (1998).
- [69] V. Greco, C. M. Ko and P. Levai, Phys. Rev. Lett. **90**, 202302 (2003).
- [70] Z. W. Lin, C. M. Ko, B. A. Li, B. Zhang and S. Pal, Phys. Rev. C **72**, 064901 (2005).
- [71] R. J. Fries, B. Muller, C. Nonaka and S. A. Bass, Phys. Rev. Lett. **90**, 202303 (2003).
- [72] R. J. Fries, B. Muller, C. Nonaka and S. A. Bass, Phys. Rev. C **68**, 044902 (2003).
- [73] V. Greco, C. M. Ko and P. Levai, Phys. Rev. C **68**, 034904 (2003).
- [74] C. Loizides, J. Kamin and D. d'Enterria, Phys. Rev. C **97**, 054910 (2018) [erratum: Phys. Rev. C **99**, 019901 (2019)].
- [75] S. Tripathy, S. De, M. Younus and R. Sahoo, Phys. Rev. C **98**, 064904 (2018).